## PCCP



PAPER View Article Online



Cite this: Phys. Chem. Chem. Phys., 2023, **25**, 21993

# Temperature dependence of radiative and non-radiative decay in the luminescence of one-dimensional pyridinium lead halide hybrids†

Abdulrahman M. Alfaraidi, Jonas Schaab, Eric T. McClure, Michael Kellogg, Taylor L. Hodgkins, Muazzam Idris, Stephen E. Bradforth, Brent C. Melot, \*\*Mark E. Thompson\*\* and Peter I. Djurovich\*\*

The photoluminescence properties of organic-inorganic pyridinium lead bromide [(pyH)PbBr $_3$ ] and iodide [(pyH)Pbl<sub>3</sub>] compounds were investigated as a function of temperature. The inorganic substructure consists of face-sharing chains of PbX<sub>6</sub> octahedra. Diffuse reflectance spectra of the compounds show low energy absorption features consistent with charge transfer transitions from the PbX<sub>3</sub> chains to the pyridinium cations. Both compounds display extremely weak luminescence at room temperature that becomes strongly enhanced upon cooling to 77 K. Broad, featureless low energy emission  $(\lambda_{\rm em}>600~{\rm nm})$  in both compounds have large Stokes shifts [1.1 eV for (pyH)PbBr<sub>3</sub> and 0.46 eV for (pyH)PbI<sub>3</sub>] and are assigned to transitions from self-trapped excitons on the inorganic chains whereas emission at higher energy in (pyH)PbBr $_3$  ( $\lambda_{em}=450$  nm) is assigned to luminescence from a free exciton state. Analysis of data from temperature-dependent luminescence intensity measurements gives activation energies  $(E_a)$  for non-radiative decay of the self-trapped excitons in  $(pyH)PbBr_3$  and  $(pyH)Pbl_3$ ,  $(E_a = 0.077 \text{ eV} \text{ and } 0.103 \text{ eV}, \text{ respectively})$  and for the free exciton in (pyH)PbBr<sub>3</sub>  $(E_a = 0.010 \text{ eV})$ . Analysis of temperature dependent luminescence lifetime data indicates another non-radiative decay process in  $(pyH)PbI_3$  at higher temperatures ( $E_a = 0.17$  eV). A large increase in the luminescence lifetime of (pyH)Pbl<sub>3</sub> below 80 K is consistent with thermalization between triplet sublevels. Analysis of the luminescence power dependence for (pyH)PbI<sub>3</sub> shows superlinear response suggestive of quenching by static traps.

Received 12th May 2023, Accepted 1st August 2023

DOI: 10.1039/d3cp02186f

rsc.li/pccp

#### Introduction

Organic–inorganic metal halide perovskite hybrid materials have emerged as the new frontier in the field of optical and electronic applications. Three-dimensional (3D) perovskites of this type possess the general formula of ABX<sub>3</sub>, in which A is a large inorganic cation like Cs<sup>+</sup> or a small organic cation like CH<sub>3</sub>NH<sub>3</sub><sup>+</sup>, and B is a divalent metal like Pb<sup>2+</sup> or Sn<sup>2+</sup>, whereas X is a halogen (Cl<sup>-</sup>, Br<sup>-</sup>, and I<sup>-</sup>). The 3D networked perovskites, where the A cations fill voids in the octahedral anions BX<sub>6</sub>, have been studied extensively in the past decades due to their excellent performance in photovoltaics and light-emitting

rich library of materials that can be synthesized using diverse organic and inorganic components.<sup>8,9</sup>

Low-dimensional organic-inorganic hybrid materials exhibit interesting broadband luminescence with large Stokes shifts, which is facilitated through strong exciton localization effects.<sup>10,11</sup>

interesting broadband luminescence with large Stokes shifts, which is facilitated through strong exciton localization effects. his facilitated through strong exciton localization effects. has been attributed to strong interaction of excitons with lattice vibrations, forming self-trapped excitons (STEs). Such phenomena can induce lattice deformation of crystals creating self-trapped subband gap states that can act as luminescent centers. Self-trapped states are in thermal equilibrium with delocalized electronic states, separated by activation energies that vary depending on the dimensionality of the material. Notably, 1D hybrids have a low energy barrier between self-trapped and free excitons (FE), allowing quick tunneling from delocalized states to trapped states. This behavior was shown experimentally in

diodes (LEDs).<sup>6,7</sup> Moreover, lower-dimensional hybrids, in which

charge carriers are bound within metal halide sheets (2D), chains

(1D), or isolated octahedra (0D) have attracted attention due to

their strong dielectric and quantum confinement as well as the

Department of Chemistry, University of Southern California, Los Angeles, CA, 90802, USA. E-mail: melot@usc.edu, met@usc.edu, djurovic@usc.edu

† Electronic supplementary information (ESI) available: Energy band structure calculated for (pyH)PbBr<sub>3</sub> and (pyH)PbI<sub>3</sub>, analysis of temperature dependent luminescence spectra intensities and linewidths for (pyH)PbBr<sub>3</sub> and (pyH)PbI<sub>3</sub>, tables with powder X-ray data collection parameters and fit parameters for luminescence power dependence data from (pyH)PbI<sub>3</sub> and aluminum quinolate (AlQ<sub>3</sub>). See DOI: https://doi.org/10.1039/d3cp02186f

**Paper** 

several reported 1D hybrids, in which emission from high energy free exitonic states coexist with broad, low energy features associated with STEs. 19,20 It is noteworthy that most of the studies on luminescence of low-dimensional hybrids have treated the organic cation as a structure-directing agent, focusing only on the inorganic moieties and their geometric distortions as an explanation for photoluminescence. However, a few reports have shown that conjugated organic molecules can also contribute to the emission when the organic frontier molecular orbitals overlap with self-trapped states.21-24 Hence, understanding the interaction between organic and inorganic moieties can facilitate better strategies for engineering materials with improved photoluminescence properties for applications

such as light down-converters or LEDs.

Here, we investigate the photophysical properties of onedimensional pyridinium lead halides [(pyH)PbX<sub>3</sub>]. The aromatic pyridinium cation was shown to yield a 1D inorganic motif with face-shared chains of PbX<sub>6</sub> octahedra. 25,26 This motivated us to study the photoluminescence behavior of the 1D (pyH)PbBr3 and (pyH)PbI<sub>3</sub> chains. The photophysical properties of these derivatives at low temperature have been recently examined by others. 27-33 The temperature-dependent steady-state photoluminescence (PL) studies show that both compounds exhibit intrinsic low-temperature emission originating from self-trapped states. Our investigation supports this interpretation of the luminescence while also including analysis of emission decay kinetics and power-dependent PL intensity measurements to further characterize the photophysical properties of these materials.

### **Experimental**

After preliminary solubility experiments, a hydrothermal synthesis method was adopted that was used for all subsequent data collection in this work. Pyridinium halide salts were prepared by the dropwise addition of stoichiometric amounts of concentrated hydrohalic acids to an ethanolic pyridine solution in an ice bath. After the acid-base neutralization, the solution was heated to dryness on a hotplate resulting in a colorless powder of the pyridinium salt. To prepare (pyH)PbBr<sub>3</sub> a 23 mL Teflon liner was charged with PbBr<sub>2</sub> (0.734 g, 2 mmol) followed by 5 mL of 8.84 M HBr and stirred. Solid pyHBr (0.320 g, 2 mmol) was then added and the solution was stirred a few more minutes before removing the stir bar and sealing the liner inside of a stainless-steel autoclave. An identical procedure was employed to prepare (pyH)PbI<sub>3</sub> using PbI<sub>2</sub> (0.461 g, 1 mmol), 7.58 M HI (10 mL) and pyHI (0.207 g, 1 mmol). The reaction vessels were heated from room temperature to 150 °C over two hours, held at 150 °C for six hours and then cooled back to room temperature at a rate of 2 °C h<sup>-1</sup>. The materials were recovered by vacuum filtration on a fritted funnel and stored under vacuum at room temperature. This reaction typically produced several large yellow-orange needles for (pyH)PbI<sub>3</sub> (the largest on the order two centimeters long) and aggregates of colorless needles for (pyH)PbBr3 (typically less than 2 millimeters long). The compounds are stable to ambient conditions and were stored in a desiccator prior to analysis.

Laboratory X-ray powder diffraction was collected on a Bruker D8 Advance diffractometer equipped with a Cu Kα source ( $\lambda_1 = 1.5406 \text{ Å}$ ,  $\lambda_2 = 1.5444 \text{ Å}$ ). The optical properties of the ground crystals were characterized using a PerkinElmer UVvis-NIR Lambda 950 in a diffuse reflectance geometry after mixing into a MgO matrix at a 3 wt % concentration.

Electronic band structure, density of states (DOS), and optical absorption calculations were calculated using density functional theory as implemented in the Vienna Ab initio Simulation Package (VASP; v6.2.0).34-37 PBEsol38 was used as the exchange correlation functional for geometric optimization while spin-orbit coupling (SOC) was added for initial DOS and band structure calculations. The hybrid functional HSE06 (incorporating a 25% Hartree-Fock exchange and a screening parameter of 0.207  $\text{Å}^{-1}$ )<sup>39</sup> with the addition of spin-orbit coupling was used for final optical absorption and DOS calculations. No adjustments were made to the exchange 'alpha' parameter to force a match of the DFT gap to experimental values. Valence and core electron interactions were accounted for within the projector-augmented wave (PAW) method (Pb\_d, I, Br, H, C, N). 40 A cutoff energy of 600 eV and a k-mesh of  $1 \times 2 \times$ 2 were used for all calculations, and the structures were considered relaxed when the forces did not exceed 0.01  $\mathring{A}^{-1}$  on each atom. Setting up, executing, and post-processing of VASP calculations utilized the pymatgen, 41 atomic simulation environment, 42 and sumo<sup>43</sup> packages.

Luminescence studies were performed on powder samples that were sandwiched between two sapphire substrates. Photoluminescent emission spectra were recorded using a Photon Technology International QuantaMaster model C-60 spectrofluorometer. Measurements in the range of 3-320 K were performed using a Janis model SHI-4-2 optical He cryostat equipped with a Lakeshore model 335 temperature controller. Steady state excitation was performed using either a 325 nm or 375 nm LED source for (pyH)PbBr3 and (pyH)PbI3, respectively. Emission decay lifetimes for (pyH)PbI3 were determined by the time-correlated single-photon counting method (TCSPC) using an IBH Fluorocube instrument using a 405 nm pulsed laser diode.

The excitation source for the power dependent measurements was an Alphalas-Pulselas-A Nd:YAG variable repetition rate laser with an internal trigger. The repetition rate was set at 10 kHz. The fundamental of the laser at 1064 nm was frequency doubled to 532 nm. The residual fundamental and its second harmonic were steered by two periscope mirrors and then focused with a 5 cm lens into a 1 cm long sum frequency crystal to generate the third harmonic, 355 nm. The output was then recollimated by a 7 cm lens and the 355 nm separated from the other colors using a fused silica prism. A USB2000 spectrometer was used to characterize the 355 nm. A variable, reflective, neutral density (ND) filter wheel was then used to attenuate the UV light for the power dependence study. The 355 nm was focused onto a PCU600-1-SS-HP from Multimode Fiber Optics, Inc. This is a single mode, 600-micron diameter, 1 m long, flexible silica core fiber. The light is attenuated by 2% when passing down this fiber. The output of the fiber optic was coupled to a 1.2 cm focal length lens used to illuminate the

sample chamber. The laser power was measured with a Newport Multi-Function Optical Meter, Model 1835-C power meter with a Newport Model 818-UV power head. The maximum power of the 355 nm achieved was 330 µW, emerging from the end of the fiber. The illumination power was measured after transmission down the fiber to account for any transmission loss. The illumination spot size at the sample was measured to be 4 mm, equivalent to a maximum light intensity of 2.6 mW cm<sup>-2</sup>. Data collection took place as follows: the ND filter wheel was rotated; the power was measured, and the emission spectrum was collected.

The luminescence for the power dependence measurements was collected in the following way. The emission from the sample was collected outside the cryostat using a system of two lenses. Both lenses were plano-convex, 5.0 cm in diameter, and manufactured from N-BK7 glass with anti-reflection coating for light from 350 to 700 nm. The first lens in this imaging system was an Edmund Optics 7.5 cm focal length lens which was used to collimate the emission. The recollimated light was then sent to the second lens of the collection system, a 12.5 cm focal length lens, which focused the emission light onto the detection fiber. The detection fiber used was a Thorlabs bifurcated, 19 fiber bundle fiber optic with each core having a diameter of 200 µm. The leg with 9 fibers was used to send light to the fluorimeter for emission detection while the leg with the other 10 fibers were not used in these sets of experiments. The fluorimeter used was a QuantaMaster model C-60 spectrofluorometer. A 355 nm notch filter was placed in front of the detection monochromator to reject any scattered laser light. The slit widths in the emission detection monochromator were set at 10 nm to increase signal to noise ratio, appropriate as the spectrum has a single broad peak. The integration time for each 5 nm increment was set at 500 ms. For each power, the emission spectrum was collected and averaged 10 times.

#### Results and discussion

The hybrid organic-inorganic materials were prepared using methods similar to those reported elsewhere<sup>26</sup> to obtain the

compounds as colorless [(pyH)PbBr<sub>3</sub>] and yellow-orange [(pyH)PbI<sub>3</sub>] powders. Samples were analyzed by X-ray powder diffraction (XRPD), which indicated a phase pure sample of (pyH)PbI<sub>3</sub>, but the bromide analog contained reflections that do not belong to the target composition. This was seen previously by Selivanov et al., who reported the presence of additional reflections in the powder patterns that were not observed in single crystal samples.<sup>26</sup> We were not able to ascribe the additional reflections to the reagent salts (pyHBr, PbBr<sub>3</sub>) or another simple known ternary phase. A pattern fit for the bromide sample (shown in Fig. 1(a)) agrees with the reported cell parameters, allowing for thermal expansion. Nevertheless, the presence of impurities in these samples means that interpretation of the photophysical properties for [(pyH)PbBr<sub>3</sub>], particularly the luminescence data, should be viewed with caution despite being similar to closely related face-sharing 1D hybrid lead bromide derivatives. 20,28 Meanwhile, the diffraction of the iodide sample permitted a Rietveld refinement (Fig. 1(b)) for (pyH)PbI<sub>3</sub> which shows excellent agreement with the reported structure save for temperature differences. A table summarizing the derived structural parameters is given in the ESI† (Table S1).

The optical absorption spectra of both compounds were experimentally obtained from Kubelka-Munk transformation of the diffuse reflectance data (Fig. 2(a)). The onset of the absorption spectrum for (pyH)PbBr3 is at 360 nm (3.44 eV) and peaks at 315 nm (3.94 eV) before rising sharply at energies > 280 nm (4.43 eV). For (pyH)PbI<sub>3</sub> the absorption onset is at 520 nm (2.38 eV) followed by a peak at 400 nm (3.1 eV) and a sharp rise at 275 nm (4.50 eV). The pyridinium molecule is expected to absorb at 265 nm, 44 thus the absorption bands at  $\lambda < 280$  nm are assigned to  $\pi$ - $\pi^*$  transitions on the pyridinium cation. The peaks at 315 and 400 nm in the respective bromide and iodide compounds are assigned to transitions in the lead halide chains on the basis of comparison to spectra from analogous face-sharing 1D lead halide materials. 20,28,45-48 These bands are bathochromically shifted from the lowest energy Pb(6s)-Br(4p)/I(5p) to Pb(6p) transitions in the respective 0D structures Cs<sub>4</sub>PbBr<sub>6</sub> (310 nm, 4.0 eV) and Cs<sub>4</sub>PbI<sub>6</sub> (3.4 eV).<sup>49</sup> Absorption features at the onsets are

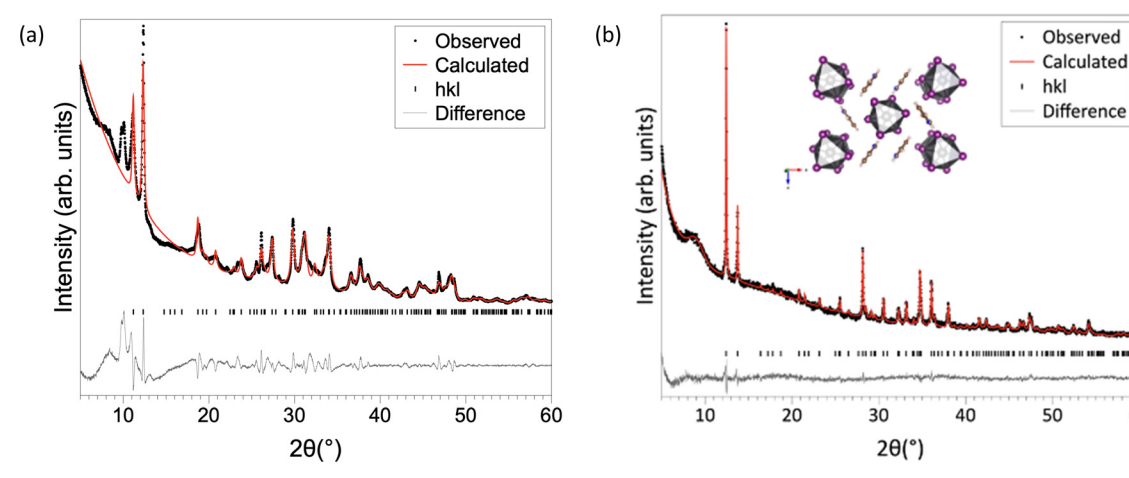


Fig. 1 (a) Calculated fit to XRPD data for (pyH)PbBr<sub>3</sub>. (b) Rietveld fit to XRPD data for (pyH)PbI<sub>3</sub> along with a packing diagram of the compound viewed down the b-axis.

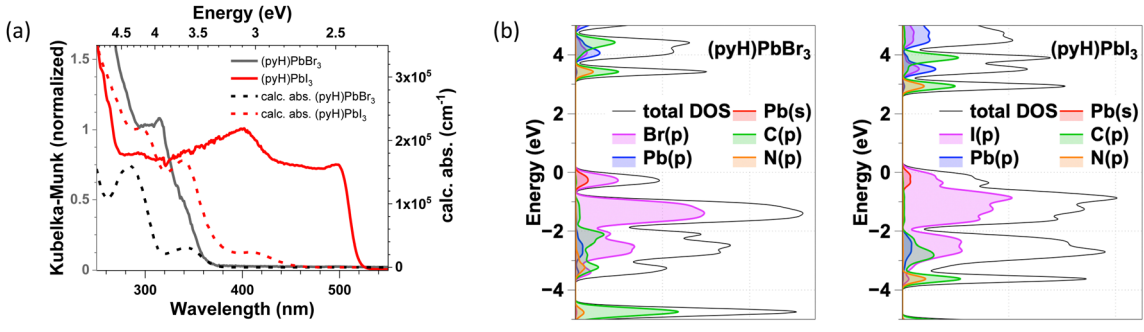


Fig. 2 (a) Kubelka-Munk transformation of the diffuse reflectance data along with calculated spectra for (pyH)PbBr<sub>3</sub> and (pyH)PbI<sub>3</sub>. (b) Density of state diagrams calculated for (pyH)PbBr3 and (pyH)PbI3.

assigned to lead-halide-to-pyridinium charge transfer (CT) transitions based on DFT calculations of the electronic density of states shown in Fig. 2(b). The absence of a high energy transition for the pyridinium ion has been cited as evidence that the low energy band is a CT transition;<sup>26</sup> however, this is not always the case. 14 We therefore assign the low energy transitions to CT states even though we clearly see the pyridinium band in the UV spectra. The calculations show valence bands comprised of Pb(6s) and Br(4p)/I(5p) orbitals, whereas the lowest energy conduction band orbitals are localized on the pyridinium cations (Fig. 2(b)). Energy bands with carbon and nitrogen character assigned to the pyridinium ions appear ca. 0.6 eV lower than the conduction bands with orbitals on the lead halides. These results agree with the energy difference between the onset of absorption and transitions on the inorganic chains as well as with previously published DFT calculations of the same compounds.26 The presence of a distinct CT absorption band in (pyH)PbI3 at low energy is due to effective spatial overlap between the iodide ions and empty 2p-orbitals on the pyridinium cations, whereas the equivalent transition occurs at higher energy in (pyH)PbBr<sub>3</sub> owing to the greater ionization energy required to oxidize the lead bromide chain.

The steady-state luminescence properties of (pyH)PbBr<sub>3</sub> and (pyH)PbI<sub>3</sub> were investigated as a function of temperature. Extremely weak orange emission ( $\Phi_{\rm PL}$  < 0.1%) is observed upon excitation of (pyH)PbBr<sub>3</sub> ( $\lambda_{ex} = 325$  nm) and (pyH)PbI<sub>3</sub>

 $(\lambda_{\rm ex}$  = 370 nm) at room temperature. Upon cooling to 80 K this luminescence band narrows, blue shifts and strongly increases in intensity, becoming a well-defined band at 660 nm (1.88 eV) for (pyH)PbBr<sub>3</sub> and 620 nm (2.00 eV) for (pyH)PbI<sub>3</sub> (Fig. 3). The blue shift in emission upon cooling occurs from transitions returning to vibronic levels in the ground state that are no longer thermally activated to higher energy as they would be at elevated temperatures. Upon further cooling down to 3 K the emission bands remain at the same energy but decrease in intensity. The full-width half maximum (fwhm) for the bands at 80 K is 0.34 eV and 0.29 eV for (pyH)PbBr3 and (pyH)PbI3, respectively. In addition, a new emission band also appears in (pyH)PbBr<sub>3</sub> at 450 nm (2.78 eV) below 80 K (Fig. 3(a)). This emission band is narrower (fwhm = 0.23 eV at 3 K) than the band at lower energy and continuously increases in intensity on cooling to 3 K. We have not been able to observe an equivalent luminescence feature at high energy from samples of (pyH)PbI<sub>3</sub>.

The photoluminescence excitation (PLE) spectra for the low energy emission bands from (pyH)PbBr<sub>3</sub> and (pyH)PbI<sub>3</sub> at 77 K are shown in Fig. 4. The onset of the PLE spectrum for (pyH)PbBr<sub>3</sub> occurs at an energy that is close to the absorption edge seen in the diffuse reflectance spectrum at room temperature and the emission shows a marked red shift relative to the PLE maximum. In contrast, for (pyH)PbI3 the onset of the PLE spectrum is at a higher energy than seen in the absorption (diffuse reflectance)

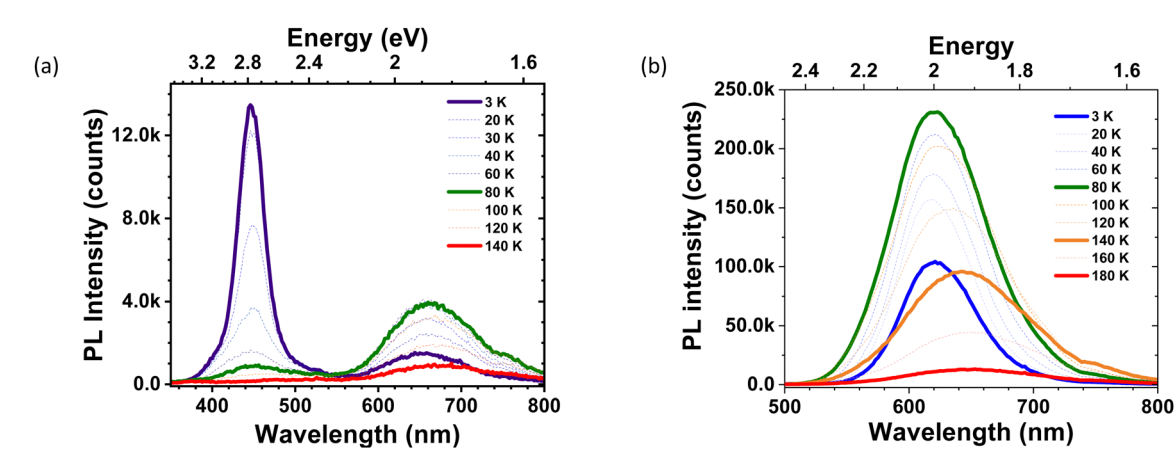


Fig. 3 Temperature-dependent steady-state photoluminescence spectra of (a)  $(pyH)PbBr_3$  ( $\lambda_{ex} = 325$  nm) and (b)  $(pyH)Pbl_3$  ( $\lambda_{ex} = 375$  nm).

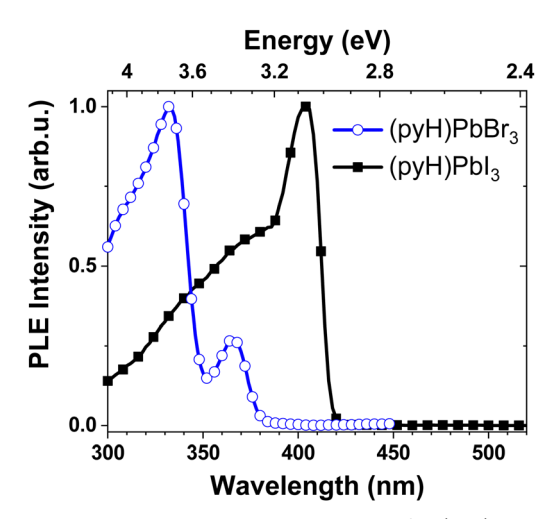


Fig. 4 Photoluminescence excitation spectrum for (pyH)PbBr<sub>3</sub> ( $\lambda_{em}$  = 660 nm) (pyH)PbI<sub>3</sub> ( $\lambda_{em}$  = 620 nm) at 77 K.

spectrum recorded at room temperature, which is consistent with a blue shift in energy upon cooling reported previously for this compound.<sup>27</sup> The distinct response to temperature is likely due to structural reorganization that occurs upon cooling. The excitation spectrum does not show any sub-band gap features, which is consistent with permanent defects not being the origin of the emission. The large energy shift between the maxima in the PLE and emission spectra for both (pyH)PbBr<sub>3</sub> and (pyH)PbI<sub>3</sub>  $(\Delta E = 1.5 \text{ and } 1.1 \text{ eV}, \text{ respectively})$  is indicative of a large structural reorganization in the excited state, consistent with emission from a self-trapped exciton.

The strong temperature dependence in the intensity and peak width for the PL profiles of both materials displayed in Fig. 3 are a common phenomenon observed in luminescence transitions caused by STEs. The luminescence behavior at low temperatures in (pyH)PbBr3 is in partial agreement with luminescence spectra reported previously for face-sharing 1D leadhalide hybrids. 20,47 The broad luminescence at low energy can be assigned to emission from an STE based on the large Stokes shift and microsecond emission lifetime at 80 K ( $\tau = 2.1 \mu s$ ).<sup>50</sup> Emission from STEs in other 1D PbBr<sub>3</sub> hybrids appear at similar wavelengths and strongly increase in intensity at low temperatures. The luminescence band at higher energy has also been reported to appear in PbBr<sub>3</sub> hybrid materials at low temperatures, although it is not observed in all samples. The high energy peak in the PL spectrum of (pyH)PbBr<sub>3</sub> decays with a lifetime of 19.8 ns at 80 K, which agrees with fast radiative recombination of the free exciton.51 The temperature-dependent PL behavior has been ascribed to coexistence of free and self-trapped excitons being responsible for the emission at high and low energy, respectively.20,51 The electron-phonon interaction is weaker in the free exciton than in the STE as evidenced by the narrower linewidth in the former emissive transition. At temperatures below 80 K, the free excitons have insufficient energy to overcome an energy barrier to the STE state, leading to higher intensity for the low energy peak with decreasing temperature. Apparently, the energy barrier required to form the STEs in (pyH)PbI3 is so small,

or even nonexistent, that emission from free excitons is not observed, even at temperatures down to 3 K. Emission bands at 450 nm have been reported at low temperatures in studies of other 1D lead bromide hybrid materials that utilized a variety of imidazolyl cations. 45,46 Likewise, a narrow emission band at 520 nm (2.38 eV) has been reported in the luminescence spectrum of (pyH)PbBr<sub>3</sub> at 77 K.<sup>28</sup> The luminescence bands in these materials have been assigned either to fluorescence from the imidazolyl or to CT transitions from the PbBr<sub>3</sub> chain to the pyridinium cation. However, since the same emission feature appears in PbBr<sub>3</sub> hybrids using piperidinium ( $\lambda_{max} = 420 \text{ nm}$ )<sup>47</sup> and other saturated amines ( $\lambda_{\text{max}} = 450 \text{ nm}$ ),  $^{20,53}$  a more consistent assignment for this transition is luminescence from a free exciton.

The changes in the intensity and line shape of the luminescence spectra upon cooling the (pyH)PbX3 compounds parallel data reported for other 1D PbBr<sub>3</sub> hybrids<sup>20</sup> as well as spectra recently reported for (pyH)PbI<sub>3</sub><sup>27</sup> and the structurally analogous piperidinium-PbI<sub>3</sub> hybrid ( $\lambda_{\text{max}} = 590 \text{ nm}$ ) (Fig. S2-S6, ESI†).<sup>48</sup> The emission features at low energy in these 1D inorganic chains has also been attributed to the formation of chargeseparated polaron pair STEs that facilitate the emergence of self-trapped states. 47 The large decrease in the luminescence intensity upon increasing the temperature above 80 K indicates the presence of energy barrier required for structural arrangement and deactivation of the excited state. The thermal activation energy  $(E_a)$  for non-radiative decay can be extracted by fitting the integrated intensities of the low energy emission above 80 K to a modified Arrhenius formula  $(eqn (1))^{47,52}$ 

$$I = \frac{I_0}{\left(1 + Ae^{\left(\frac{-E_a}{k_B T}\right)}\right)} \tag{1}$$

where  $I_0$  is the integrated emission at highest intensity. This analysis assumes only a single process is responsible for nonradiative decay.<sup>52</sup> Activation energies for the emission using egn (1) were found from fits to the luminescence intensity data in Fig. 3 for the low energy emission at T > 80 K (Fig. S2, S3 and S5, ESI†). The values obtained for (pyH)PbBr<sub>3</sub> ( $E_a = 0.077 \text{ eV}$ ) and (pyH)PbI<sub>3</sub> ( $E_a = 0.103$  eV) are comparable to  $3k_BT$  at room temperature (0.078 eV). This energy barrier is likely tied to molecular motions that are frozen out at low temperatures.<sup>27</sup> Such low activation energies explain the effective suppression of emission intensity at room temperature in both materials. Furthermore, a similar analysis for the high energy transition in (pyH)PbBr3 determined the activation energy for non-radiative decay of the free exciton state ( $E_a = 0.0104$  eV). This activation energy likely represents the phonon assisted conversion of the free exciton into the STE.27

The emission intensity for (pyH)PbBr<sub>3</sub> was too low at cryogenic temperatures for us to be able to measure the decay lifetimes using our system. However, the transient lifetimes for emission decay for (pyH)PbI3 could be investigated in the temperature range of 3-290 K (Fig. 5). Analysis of luminescence decay rates can provide a more detailed picture of the excited

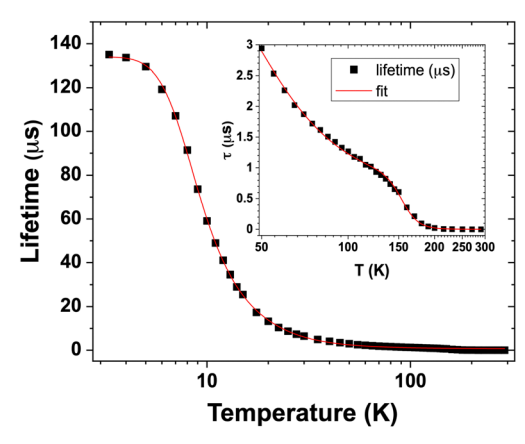


Fig. 5 Temperature dependent lifetime data for (pyH)PbI<sub>3</sub> ( $\lambda_{em}$  = 620 nm) along with Boltzmann fits to the data. Inset shows data in the higher temperature range

state properties than from data obtained solely by changes in the luminescence intensity. Average lifetimes were found to increase from 0.5 ns to 2.1 µs upon cooling from 290 to 80 K with an inflection point at 170 K. The lifetimes continue to increase on further cooling and rise sharply at 20 K before plateauing at 3 K ( $\tau$  = 135  $\mu$ s). The inflection points at different temperature regimes suggest different thermally activated mechanisms are operative in this compound. Activation energies can be obtained by fits to the data using a multi-term Boltzmann equation (eqn (2)):

$$\tau = \frac{1 + e^{-\frac{\Delta E_{a1}}{k_B T}} + e^{-\frac{\Delta E_{a2}}{k_B T}}}{A_0 + A_1 e^{-\frac{\Delta E_{a1}}{k_B T}} + A_2 e^{-\frac{\Delta E_{a2}}{k_B T}}}$$
(2)

A fit to the complete data set does not accurately account for small changes in lifetimes at temperatures above 100 K as such a fit is weighed disproportionately to the large changes in lifetimes that occur at temperatures below 50 K. Therefore, a fit was first performed on the full data set to obtain  $E_{a1}$ ,  $E_{a2}$ ,  $A_0$ ,  $A_1$  and  $A_2$  followed by a second fit of data between 50-300 K using parameters obtained from the initial analysis to obtain an additional set of values for  $E_{a3}$  and  $A_3$ . Values for the activation energies and pre-exponentials obtained from the fits are shown in Table 1. The concurrent increase in luminescence intensity and lifetime upon cooling to 80 K suggest that decay from thermally activated non-radiative states controls the emission process at high temperatures. Enhanced molecular vibrations and reorientations of the pyridinium cation have been proposed as a mechanism that promotes non-radiative decay at these temperatures.<sup>27</sup> Increases in the disorder among pyridinium dipole moments will then promote the observed bathochromic shifts and line-broadening of the emission band. The activation energy for this process using lifetime data ( $E_{a3} = 0.17$  eV, inset to Fig. 5) is comparable to the one-parameter fit obtained from the emission intensity using eqn (1) and consistent with a phase transition that has been observed in (pyH)PbI<sub>3</sub> at 170 K using heat capacity and single crystal X-ray diffraction measurements.<sup>27</sup> Cooling below this temperature leads to an decrease in disorder

Table 1 Activation energies and pre-exponential terms obtained from fits of temperature dependent data to eqn (2)

$E_{a1}$ (eV)	$E_{\rm a2}$ (eV)	$E_{a3}$ (eV)	$A_0$ ( $\mu$ s)	$A_1$ ( $\mu$ s)	$A_2$ ( $\mu$ s)	$A_3$ ( $\mu$ s)
0.0032	0.010	0.17	134	2.5	0.21	$1.5 \times 10^{-6}$

of the pyridinium cations akin to freezing that inhibits the extremely rapid deactivation of the excited state as indicated by the magnitude of the decay rate  $(A_3 = 1.5 \times 10^{-6} \, \mu s)$ . The data suggests that molecular disorder increases at high temperatures and allows sufficient distortion to promote rapid surface crossing of the STE to the ground state.

The emission lifetime increases markedly upon further cooling below 80 K despite a decrease in emission intensity which indicates a thermally activated change in the radiative rate. Such changes in the radiative rates at cryogenic temperatures are consistent with emission decay from individual sublevels of the emissive triplet state. These sublevels have characteristic emission lifetimes that are independent of temperature and are shifted to different energies by zero field splitting (ZFS) induced by asymmetries in the molecular structure. A tetragonal distortion observed in the PbX<sub>6</sub><sup>2-</sup> octahedra will remove the degeneracy of the triplet state and split it into two low-lying sublevels (T<sub>I</sub> and T<sub>II</sub>) and one lying at higher energy  $(T_{III})^{54}$  In this model the values of  $E_{a1}$  and  $E_{a2}$  represent the energy splitting between the T<sub>I</sub>-T<sub>II</sub> and T<sub>I</sub>-T<sub>III</sub> sublevels, whereas  $A_0$ ,  $A_1$  and  $A_2$  are the decay rates from  $T_I$ ,  $T_{II}$  and  $T_{III}$ , respectively. The ZFS ( $E_{a2}$  = 0.010 eV) and decay rates determined from analysis of the lifetime data are comparable to values found for other heavy metal complexes.<sup>55</sup> The values for the decay rate from  $T_{I}$  ( $A_0 = 134 \mu s$ ) and  $T_{II}$  ( $A_1 = 2.5 \mu s$ ) are also in a similar range of values as observed for 1D (piperidinium)PbBr<sub>3</sub>. 47 The rapid decay rate from the highest triplet sublevel ( $A_2 = 0.21 \mu s$ ) indicates strong mixing of singlet character into the triplet state induced by spin-orbit coupling from the heavy Pb and I ions. The discussion here is built around the picture of an excited state triplet. A similar picture involving distinct LS coupled states could also be used to explain the lifetime analysis presented above.

The decrease in luminescence intensity in (pyH)PbI<sub>3</sub> observed at T < 80 K is only partially due to a decrease in the radiative rate, which indicates that other temperature dependent non-radiative processes are active in the material. Additional non-radiative channels could be caused by second order processes such as exciton-exciton and/or exciton-polaron annihilation as these mechanisms become favored when slower radiative rates allow more time for the exciton to diffuse to a quenching site. 56 Therefore, power dependent PL measurements were performed to characterize the luminescence at these low temperatures. Reference data obtained from a sample of aluminum tris-quinolate (AlQ3) at room temperature gives a linear response with increasing excitation intensity (slope = 0.97). In contrast, a plot of the luminescence intensity for (pyH)PbI<sub>3</sub> as a function of excitation power recorded at 3.1 and 77 K shows two types of non-linear response (Fig. 6 and Table S2, ESI†). At low power the PL intensity is sub-linear whereas at higher irradiation intensities the intensity becomes

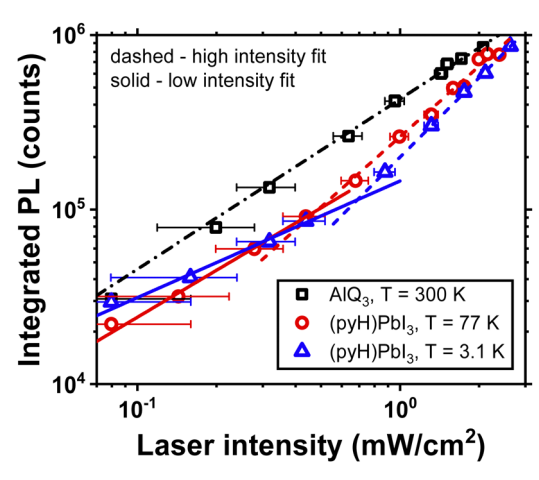


Fig. 6 Power dependent data for (pyH)Pbl<sub>3</sub> at ( $\lambda_{em}$  = 625 nm) excited with 355 nm light. The power dependent data for AlQ<sub>3</sub> ( $\lambda_{em}$  = 500 nm) is shown for reference.

super-linear. The data does not support decay of the excited state from second order processes since this would be expected to show a large variation in the power dependence of emission at the two temperatures. However, the data is consistent with a model of non-diffusive static quenching from defect sites near the STEs. In this mechanism, increasing laser power eventually saturates potential quenching sites which then leads to an increase in the luminescence intensity.

A schematic model that describes the luminescence behavior of self-trapped excitons in low dimensional hybrids is shown in Fig. 7. 13,16,57,58 The geometry of the free exciton is less distorted than that of the self-trapped exciton. A small energy barrier enables thermal activation to transform the strongly bound free excitons into the weakly bound self-trapped states, causing the broad low energy emission. However, the 1D structure allows these STEs to effectively migrate to sites where disorder among the pyridinium cations can allow thermally promoted nonradiative pathways such as surface crossing to effectively quench the intensity.<sup>59</sup> These non-radiative pathways become less accessible as the pyridinium cations "freeze" at temperatures below 200 K, evidenced by the increase of intensity of the low energy peaks, although other non-radiative processes such as migration of excitons to traps followed by vibrational tunnelling to the

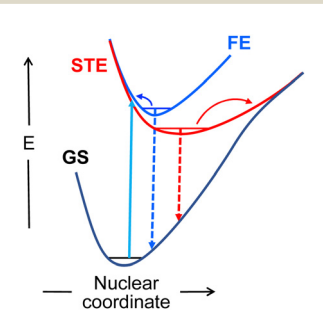


Fig. 7 Schematic potential energy surfaces for the luminescence process in (pyH)PbBr $_3$  and (pyH)PbI $_3$ . GS is ground state, STE is self-trapped exciton and FE is free exciton. Solid, dashed, and curved arrows represent absorption, emission, and thermally activated processes, respectively

ground state can still occur. Lowering the temperature further decreases the probability of excitons overcoming the energy barrier between free states and self-trapped states, which can result in an increase in the relative intensity emission from the free exciton, as observed for (pyH)PbBr3. For (pyH)PbI3 at temperatures below 80 K the radiative rate also begins to decrease, which enables non-radiative decay from vibrationally tunnelling to become competitive with emission and leads to a subsequent decrease in luminescence intensity.

#### Conclusions

The hybrid organic-inorganic compounds (pyH)PbBr<sub>3</sub> and (pyH)PbI<sub>3</sub> both luminesce strongly at low temperatures from intrinsic transitions consistent with self-trapped excitons. The luminescence is efficiently quenched at room temperature by thermally activated non-radiative decay. The poor luminescence efficiency from STEs in these one-dimensional hybrid materials can be contrasted with emission from STEs in zero-dimensional (molecular) organic-inorganic hybrids.<sup>50</sup> Luminescence from the latter compounds can be highly efficient at room temperature, suggesting that energy migration to non-radiative trap states is facile along the inorganic chain in the one-dimensional materials. Similar photophysical properties in other one-dimensional PbX<sub>3</sub> hybrids with face-sharing octrahedra<sup>60,61</sup> indicates that other structural motifs may be required to achieve efficient luminescence at room temperature from related lead halide materials.<sup>16</sup>

#### Author contributions

A. M. A., E. T. M. and T. L. H. synthesized and characterized the composition of the materials, A. M. A., J. S., E. T. M., M. K., T. L. H. and M. I. performed the spectroscopic data collection and analysis, and all authors assisted in writing the manuscript.

#### Conflicts of interest

There are no conflicts to declare.

## Acknowledgements

The authors gratefully acknowledge funding for this work under NSF Award DMR-1905826.

#### References

- 1 V. Adinolfi, W. Peng, G. Walters, O. M. Bakr and E. H. Sargent, Adv. Mater., 2018, 30, 1700764.
- 2 M. Ahmadi, T. Wu and B. Hu, Adv. Mater., 2017, 29, 1605242.
- 3 S. D. Stranks and H. J. Snaith, Nat. Nanotechnol., 2015, 10,
- 4 S. J. Adjogri and E. L. Meyer, Molecules, 2020, 25, 5039.
- 5 A. K. Jena, A. Kulkarni and T. Miyasaka, Chem. Rev., 2019, **119**, 3036-3103.

- 6 Y. H. Kim, H. Cho and T. W. Lee, *Proc. Natl. Acad. Sci. U. S. A.*, 2016, **113**, 11694–11702.
- 7 W. Y. Nie, H. H. Tsai, R. Asadpour, J. C. Blancon, A. J. Neukirch, G. Gupta, J. J. Crochet, M. Chhowalla, S. Tretiak, M. A. Alam, H. L. Wang and A. D. Mohite, *Science*, 2015, 347, 522–525.
- 8 M. I. Saidaminov, O. F. Mohammed and O. M. Bakr, *ACS Energy Lett.*, 2017, 2, 889–896.
- 9 C. K. Zhou, H. R. Lin, Q. Q. He, L. J. Xu, M. Worku, M. Chaaban, S. Lee, X. Q. Shi, M. H. Du and B. W. Ma, *Mater. Sci. Eng.*, R, 2019, 137, 38–65.
- 10 D. Cortecchia, J. Yin, A. Petrozza and C. Soci, *J. Mater. Chem. C*, 2019, 7, 4956–4969.
- 11 H. R. Lin, C. K. Zhou, Y. Tian, T. Siegrist and B. W. Ma, ACS Energy Lett., 2018, 3, 54–62.
- 12 A. Biswas, R. Bakthavatsalam, S. R. Shaikh, A. Shinde, A. Lohar, S. Jena, R. G. Gonnade and J. Kundu, *Chem. Mater.*, 2019, 31, 2253–2257.
- 13 D. Cortecchia, J. Yin, A. Bruno, S. Z. A. Lo, G. G. Gurzadyan, S. Mhaisalkar, J. L. Bredas and C. Soci, *J. Mater. Chem. C*, 2017, 5, 2771–2780.
- 14 Y. Peng, Y. P. Yao, L. N. Li, Z. Y. Wu, S. S. Wang and J. H. Luo, J. Mater. Chem. C, 2018, 6, 6033-6037.
- 15 Y. Shi, Z. W. Ma, D. L. Zhao, Y. P. Chen, Y. Cao, K. Wang, G. J. Xiao and B. Zou, J. Am. Chem. Soc., 2019, 141, 6504–6508.
- 16 Z. Yuan, C. K. Zhou, Y. Tian, Y. Shu, J. Messier, J. C. Wang, L. J. van de Burgt, K. Kountouriotis, Y. Xin, E. Holt, K. Schanze, R. Clark, T. Siegrist and B. W. Ma, *Nat. Commun.*, 2017, 8, 14051.
- 17 R. T. Williams and K. S. Song, *J. Phys. Chem. Solids*, 1990, **51**, 679–716.
- 18 V. V. Kabanov and O. Y. Mashtakov, *Phys. Rev. B: Condens. Matter Mater. Phys.*, 1993, 47, 6060–6064.
- 19 H. R. Lin, C. K. Zhou, Y. Tian, T. Besara, J. Neu, T. Siegrist, Y. Zhou, J. Bullock, K. S. Schanze, W. M. Ming, M. H. Du and B. W. Ma, *Chem. Sci.*, 2017, 8, 8400–8404.
- 20 L. L. Mao, P. J. Guo, M. Kepenekian, I. Hadar, C. Katan, J. Even, R. D. Schaller, C. C. Stoumpos and M. G. Kanatzidis, J. Am. Chem. Soc., 2018, 140, 13078–13088.
- 21 T. Dammak and Y. Abid, Opt. Mater., 2017, 66, 302-307.
- 22 K. Ema, M. Inomata, Y. Kato and H. Kunugita, *Phys. Rev. Lett.*, 2008, **100**, 257401.
- 23 G. C. Papavassiliou, G. A. Mousdis, G. Pagona, N. Karousis and M. S. Vidali, *J. Lumin.*, 2014, 149, 287–291.
- 24 A. Samet, S. Triki and Y. Abid, *J. Phys. Chem. C*, 2019, **123**, 6213–6219.
- 25 M. Geselle and H. Fuess, Z. Kristallogr. New Cryst. Struct., 1997, 212, 235.
- 26 N. I. Selivanov, A. A. Murashkina, R. Kevorkyants, A. V. Emeline and D. W. Bahnemann, *Dalton Trans.*, 2018, 47, 16313–16319.
- 27 S. Maqbool, T. Sheikh, Z. Thekkayil, S. Deswal, R. Boomishankar, A. Nag and P. Mandal, *J. Phys. Chem. C*, 2021, **125**, 22674–22683.
- 28 N. I. Selivanov, Y. A. Rozhkova, R. Kevorkyants, A. V. Emeline and D. W. Bahnemann, *Dalton Trans.*, 2020, 49, 4390–4403.
- 29 M. Z. Rahaman, S. Ge, C.-H. Lin, Y. Cui and T. Wu, *Small Struct.*, 2021, 2, 2000062.

- 30 J.-Q. Zhao, C.-Q. Jing, J.-H. Wu, W.-F. Zhang, L.-J. Feng, C.-Y. Yue and X.-W. Lei, *J. Phys. Chem. C*, 2021, **125**, 10850–10859.
- 31 Z. Qi, H. Gao, X. Yang, Y. Chen, F.-Q. Zhang, M. Qu, S.-L. Li and X.-M. Zhang, *Inorg. Chem.*, 2021, **60**, 15136–15140.
- 32 Z. Qi, Y. Chen, Y. Guo, X. Yang, H. Gao, G. Zhou, S.-L. Li and X.-M. Zhang, *Chem. Commun.*, 2021, 57, 2495–2498.
- 33 W.-F. Zhang, W.-J. Pan, T. Xu, R.-Y. Song, Y.-Y. Zhao, C.-Y. Yue and X.-W. Lei, *Inorg. Chem.*, 2020, **59**, 14085–14092.
- 34 G. Kresse and J. Furthmuller, *Comput. Mater. Sci.*, 1996, 6, 15–50.
- 35 G. Kresse and J. Furthmuller, *Phys. Rev. B: Condens. Matter Mater. Phys.*, 1996, 54, 11169–11186.
- 36 G. Kresse and J. Hafner, *Phys. Rev. B: Condens. Matter Mater. Phys.*, 1994, **49**, 14251–14269.
- 37 G. Kresse and J. Hafner, *Phys. Rev. B: Condens. Matter Mater. Phys.*, 1993, 47, 558-561.
- 38 J. P. Perdew, A. Ruzsinszky, G. I. Csonka, O. A. Vydrov, G. E. Scuseria, L. A. Constantin, X. L. Zhou and K. Burke, *Phys. Rev. Lett.*, 2008, **100**, 136406.
- 39 A. V. Krukau, O. A. Vydrov, A. F. Izmaylov and G. E. Scuseria, J. Chem. Phys., 2006, 125, 224106.
- 40 P. E. Blochl, Phys. Rev. B: Condens. Matter Mater. Phys., 1994, 50, 17953–17979.
- 41 S. P. Ong, W. D. Richards, A. Jain, G. Hautier, M. Kocher, S. Cholia, D. Gunter, V. L. Chevrier, K. A. Persson and G. Ceder, *Comput. Mater. Sci.*, 2013, 68, 314–319.
- 42 A. H. Larsen, J. J. Mortensen, J. Blomqvist, I. E. Castelli, R. Christensen, M. Dulak, J. Friis, M. N. Groves, B. Hammer, C. Hargus, E. D. Hermes, P. C. Jennings, P. B. Jensen, J. Kermode, J. R. Kitchin, E. L. Kolsbjerg, J. Kubal, K. Kaasbjerg, S. Lysgaard, J. B. Maronsson, T. Maxson, T. Olsen, L. Pastewka, A. Peterson, C. Rostgaard, J. Schiotz, O. Schutt, M. Strange, K. S. Thygesen, T. Vegge, L. Vilhelmsen, M. Walter, Z. H. Zeng and K. W. Jacobsen, J. Phys.: Condens. Matter, 2017, 29, 273002.
- 43 A. M. Ganose, A. J. Jackson and D. O. Scanlon, *J. Open Source Softw.*, 2018, 3, 717.
- 44 I. Kaljurand, UV-VIS spectra of neutral bases and their protonated conjugate cationic acids in acetonitrile, <a href="http://tera.chem.ut.ee/~manna/spe/pyridineAN.gif">http://tera.chem.ut.ee/~manna/spe/pyridineAN.gif</a>, (accessed June 2, 2022, 2022).
- 45 K. M. Wan, Y. B. Tong, L. Li, Y. Zou, H. B. Duan, J. L. Liu and X. M. Ren, *New J. Chem.*, 2016, **40**, 8664–8672.
- 46 Y. B. Tong, L. T. Ren, H. B. Duan, J. L. Liu and X. M. Ren, *Dalton Trans.*, 2015, 44, 17850–17858.
- 47 J. Azuma, K. Tanaka and K. Kan'no, *J. Phys. Soc. Jpn.*, 2002, 71, 971–977.
- 48 A. Nagami, K. Okamura and T. Ishihara, *Physica B*, 1996, 227, 346–348.
- 49 S. Kondo, A. Masaki, T. Saito and H. Asada, *Solid State Commun.*, 2002, **124**, 211–214.
- 50 V. Morad, Y. Shynkarenko, S. Yakunin, A. Brumberg, R. D. Schaller and M. V. Kovalenko, J. Am. Chem. Soc., 2019, 141, 9764–9768.
- 51 M. D. Smith and H. I. Karunadasa, *Acc. Chem. Res.*, 2018, **51**, 619–627.

- 52 Z. Chen, C. Yu, K. Shum, J. J. Wang, W. Pfenninger, N. Vockic, J. Midgley and J. T. Kenney, J. Lumin., 2012, 132, 345-349.
- 53 C. Xue, H. Huang, S. Nishihara, V. Biju, X.-M. Ren and T. Nakamura, J. Phys. Chem. Lett., 2022, 13, 7405-7412.
- 54 T. Azumi and H. Miki, Electronic and Vibronic Spectra of Transition Metal Complexes II, 1997, vol. 191, pp.1-40.
- 55 H. Yersin, A. F. Rausch, R. Czerwieniec, T. Hofbeck and T. Fischer, Coord. Chem. Rev., 2011, 255, 2622-2652.
- 56 Y.-Z. Ma, H. Lin, M.-H. Du, B. Doughty and B. Ma, J. Phys. Chem. Lett., 2018, 9, 2164-2169.
- 57 T. Hu, M. D. Smith, E. R. Dohner, M. J. Sher, X. X. Wu, M. T. Trinh, A. Fisher, J. Corbett, X. Y. Zhu, H. I. Karunadasa

- and A. M. Lindenberg, J. Phys. Chem. Lett., 2016, 7, 2258-2263.
- 58 J. C. Yu, J. T. Kong, W. Hao, X. T. Guo, H. J. He, W. R. Leow, Z. Y. Liu, P. Q. Cai, G. D. Qian, S. Z. Li, X. Y. Chen and X. D. Chen, Adv. Mater., 2019, 31, 1806385.
- 59 D. Han, H. Shi, W. Ming, C. Zhou, B. Ma, B. Saparov, Y.-Z. Ma, S. Chen and M.-H. Du, J. Mater. Chem. C, 2018, 6, 6398-6405.
- 60 H. B. Duan, S. S. Yu, Y. B. Tong, H. Zhou and X. M. Ren, Dalton Trans., 2016, 45, 4810-4818.
- 61 Y. J. She, S. P. Zhao, Z. F. Tian and X. M. Ren, Inorg. Chem. Commun., 2014, 46, 29-32.

Electronic Supplementary Material (ESI) for Physical Chemistry Chemical Physics. This journal is © the Owner Societies 2023

# **Supporting Information**

Temperature dependence of radiative and non-radiative decay in the luminescence of onedimensional pyridinium lead halide hybrids

Abdulrahman M. Alfaraidi, Jonas Schaab, Eric T. McClure, Mike Kellogg, Taylor L. Hodgkins, Muazzam Idris, Peter I. Djurovich, Stephen E. Bradforth, Brent C. Melot, Mark E. Thompson\*

Department of Chemistry, University of Southern California, Los Angeles, CA, USA

#### **Table of Contents**

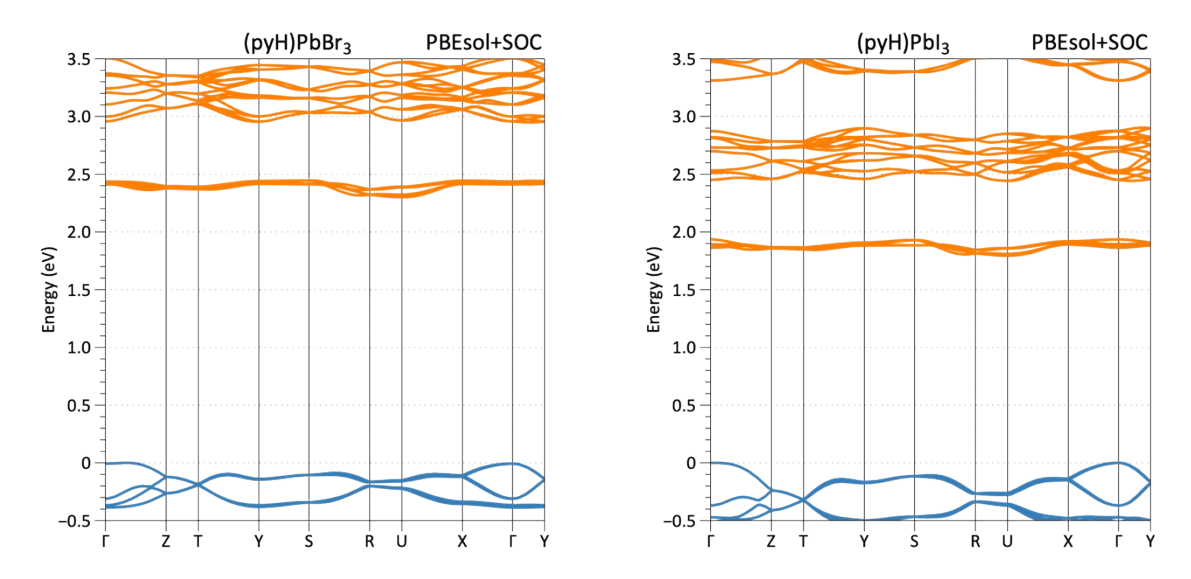
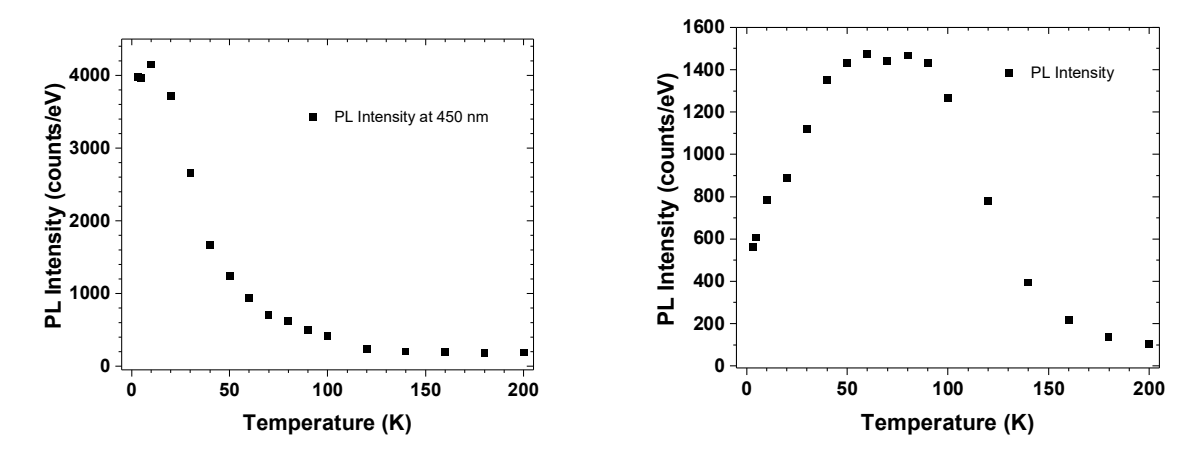
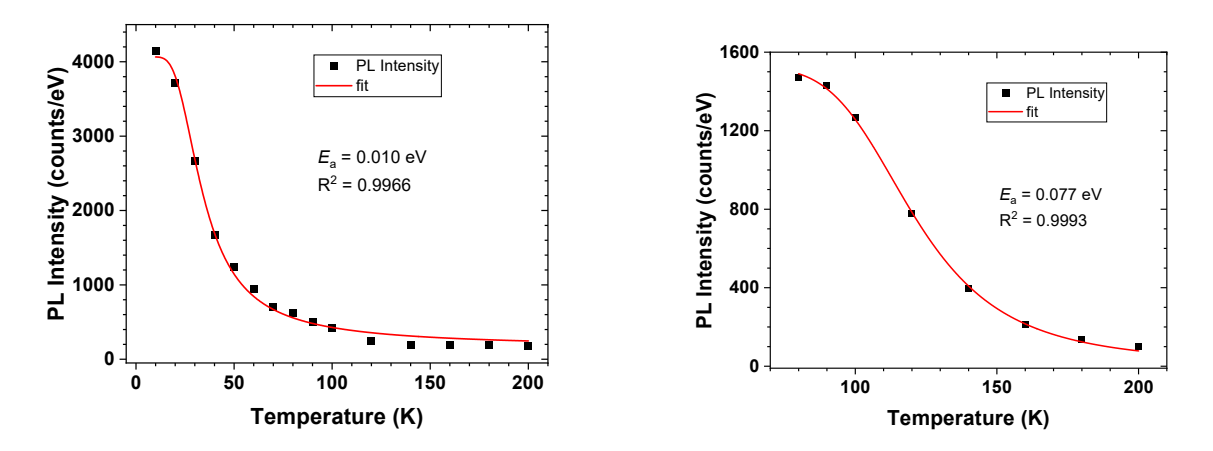


Figure S1. Band structures calculated for (pyH)PbBr<sub>3</sub> and (pyH)PbI<sub>3</sub>.



**Figure S2**. Temperature dependence of the integrated luminescence intensity for (pyH)PbBr<sub>3</sub> for emission bands at high (left) and low (right) energy.



**Figure S3**. Arrhenius fit to the temperature dependence for the low (left) and high (right) energy luminescence from (pyH)PbBr<sub>3</sub>.

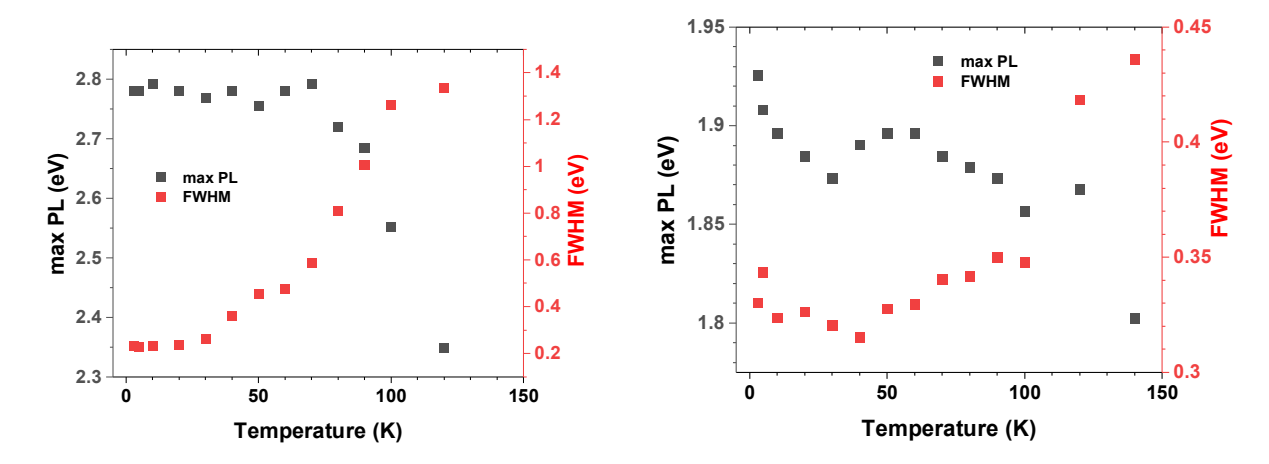


**Figure S4**. Temperature dependence of the luminescence peak maxima and linewidth at high energy (left) and low energy (right) for (pyH)PbBr<sub>3</sub>.

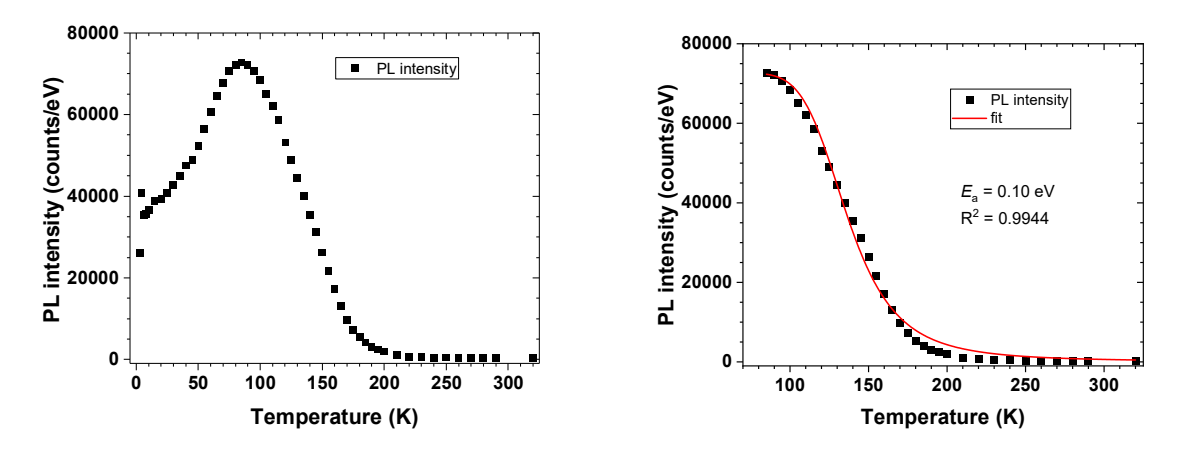
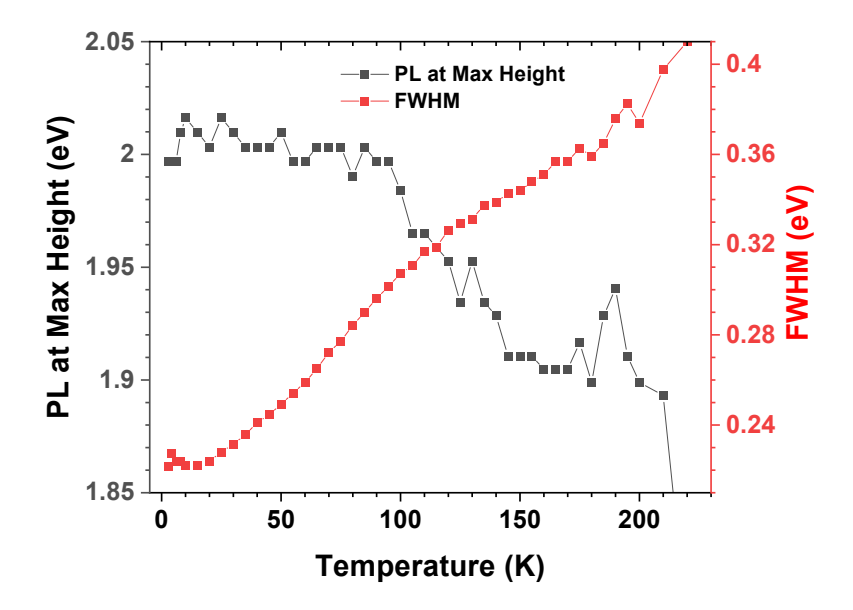


Figure S5. Temperature dependence of integrated emission intensity (left) and Arrhenius fit to the temperature dependence for the luminescence from (pyH)PbI<sub>3</sub> for T > 80 K (right).



**Figure S6**. Temperature dependence of the luminescence peak maxima and linewidth for  $(pyH)PbI_3$ .

Table S1. Powder X-ray data collection parameters for (pyH)PbBr<sub>3</sub> and (pyH)PbI<sub>3</sub>.

1 (1)	3 (1) / 3				
(pyH)PbI <sub>3</sub>	(pyH)PbBr <sub>3</sub>				
$C_5N_1H_6Pb_1I_3$	$C_5N_1H_6Pb_1Br_3$				
Pnma (#62)	Pnma (#62)				
14.9839(8)	14.348(6)				
8.1067(4)	7.740(3)				
9.9103(7)	9.474(5)				
1203.8	1052.1				
4					
Cu $K_{\alpha}$ radiation					
1.5406 / 1.5444 Å					
295 K					
0.015					
2.0					
	5–100				
5.799 (Rietveld)	7.510 (WPPF)				
	(pyH)PbI <sub>3</sub> C <sub>5</sub> N <sub>1</sub> H <sub>6</sub> Pb <sub>1</sub> I <sub>3</sub> Pnma (#62) 14.9839(8) 8.1067(4) 9.9103(7) 1203.8  Cu 1.54				

**Table S2**. Fit parameters for luminescence power dependence data from (pyH)PbI<sub>3</sub> and reference material, aluminum quinolate (AlQ<sub>3</sub>).

	<i>n</i> (low power)	a (low power)	<i>n</i> (high power)	a (high power)
(pyH)PbI <sub>3</sub> , 77 K	0.90	$1.9 \times 10^5$	1.30	$2.6 \times 10^5$
(pyH)PbI <sub>3</sub> , 3.1 K	0.67	$1.5 \times 10^5$	1.50	$2.0 \times 10^5$
AlQ <sub>3</sub> , 300 K			0.97	4.3 x 10 <sup>5</sup>

 $fit = a \cdot x^n$